Noninvasive imaging of oral premalignancy and malignancy

Petra Wilder-Smith
Tatiana Krasieva
Woong-Gyu Jung
Jun Zhang
Zhongping Chen
Katherine Osann
Bruce Tromberg
University of California
Beckman Laser Institute
Irvine, California
E-mail: pwsmith@bli.uci.edu

Abstract. Early detection of cancer and its precursors remains the best way to ensure patient survival and quality of life. Our specific aim is to test a multimodality approach to noninvasive diagnostics of oral premalignancy and malignancy. In the hamster cheek pouch model (120 hamsters), *in vivo* optical coherence tomography (OCT) and optical Doppler tomography (ODT) map epithelial, subepithelial, and vascular change throughout carcinogenesis. *In vivo* multiwavelength multiphoton (MPM) and second-harmonic generated (SHG) fluorescence techniques provided parallel data on surface and subsurface tissue structure, specifically collagen presence and structure, cellular presence, and vasculature. Images are diagnosed by two blinded, prestandardized investigators using a scale from 0 to 6 for all modalities. After sacrifice, histopathology is evaluated on a scale of 0 to 6. Imaging data are reproducibly obtained with good accuracy. Carcinogenesis-related structural and vascular changes are clearly visible to tissue depths of 2 mm. Sensitivity (OCT/ODT alone, 71 to 88%; OCT+MPM/SHG, 79 to 91%) and specificity (OCT alone, 62 to 83%; OCT+MPM/SHG, 67 to 90%) compare well with conventional techniques. Our conclusions are that OCT/ODT and MPM/SHG are promising noninvasive *in vivo* diagnostic modalities for oral dysplasia and malignancy. © *2005 Society of Photo-Optical Instrumentation Engineers.*
[DOI: 10.1117/1.2098930]

1 Introduction

According to the American Cancer Society, 1,220,100 patients were diagnosed with cancer in the year 2000. In the same year, 552,200 persons were expected to succumb to cancer.[1] Despite significant advances in cancer treatment, early detection of cancer and its curable precursors remains the best way to ensure patient survival and quality of life. Oral cancer will claim approximately 10,000 lives in the United States this year.[2,3] Of all oral cancer cases documented by the National Cancer Institute Surveillance, Epidemiology and End Results Program, advanced lesions outnumbered localized lesions more than 2:1. The 5-y survival rate is 75% for those with localized disease at diagnosis, but only 16% for those with cancer metastasis.[2,3] These data clearly indicate that, currently, most cases of oral cancer are detected far too late, and that earlier detection of these lesions would enormously improve the prognosis of these patients.

Two basic facts indicate that early detection of oral malignancy should be possible to a far greater extent:

1. Accounting for 96% of all oral cancers, squamous cell carcinoma is usually preceded by dysplasia presenting as white, red, or mixed red and white epithelial lesions on the oral mucosa (leukoplakia, erythroplakia). Leukoplakias develop in 1 to 4% of the population.[2] Malignant transformation, which is quite unpredictable, occurs in 1 to 40% of leukoplakias over 5 yr. Dysplastic lesions in the form of erythroplakias carry a risk for malignant conversion[2] of 90%. Thus, oral cancer is predominantly preceded by white or red lesions that are visible to the naked eye, and often present for a considerable period of time prior to transformation. A noninvasive diagnostic modality would enable monitoring of these lesions at regular intervals and detection of treatment needs at a very early, relatively harmless stage.

2. High-risk populations are clearly defined by tobacco use, alcohol abuse, urban environment, specific races, poor diet, and frequent exposure to sunlight.[1–4] A fast, mobile, inexpensive noninvasive diagnostic modality would enable detection of oral lesions and of treatment needs at an early, relatively harmless stage.

1.1 Existing Approaches to Diagnose Oral Premalignancy and Malignancy

1.1.1 Visual examination and biopsy

Oral cancer can be detected by dentists and physicians, but physicians do not routinely inspect their patients for suspi-

Address all correspondence to Petra Wilder-Smith, Beckman Laser Institute, University of California/Irvine, 1002 Health Sciences Rd East, Irvine, CA 92612. Tel.: (949) 824-4713; Fax: (949) 824-8413; E-mail: pwsmith@uci.edu

cious oral lesions, and dentists are also remiss in the early diagnosis and referral for oral cancer.[1–5] Since 11% of dentists and 45% of physicians do not feel adequately trained to complete an effective oral cancer examination, this results in their failure to examine for oral cancer. The current approach to detecting the transformation of leukoplakia to squamous cell carcinoma is regular surveillance combined with biopsy or surgical excision. However, visual examination provides very poor diagnostic accuracy, and biopsy techniques are invasive and unsuitable for regular screening of high-risk sectors of the population. Adequate visual identification and biopsy of all such lesions to ensure that they are all recognized and diagnosed is difficult.

Several studies have investigated use of vital staining with agents such as Lugol iodine, toluidine blue, and tolonium chloride for detection of oral malignancy.[6–11] Although the sensitivity of these agents in the hands of experts generally approximates 90%, specificity of these agents is poor; sensitivity rapidly decreases when this modality is used by nonexperts such as screeners in field units.[6–11] Extensive clinical experience is necessary to perform these examinations adequately.[6–11]

1.1.2 Photosensitizers

Topical or systemic application of chemical agents called photosensitizers can render pathologic tissues fluorescent when exposed to specific wavelengths of light.[12] While several studies have demonstrated the use of various porphyrins as photosensitizers, their accumulation in skin after systemic administration can cause phototoxic reactions upon exposure to sunlight.[13,14] An alternative approach is to stimulate synthesis of photosensitizing agents *in situ* with a photoinactive precursor. The photosensitizer, protoporphyrin IX (PpIX) is an immediate precursor of heme in the biosynthetic pathway for heme. In certain types of cells and tissues, the rate of PpIX synthesis is determined by the rate of synthesis of 5-aminolevulinic acid (ALA), which in turn is regulated via a feedback control mechanism governed by the concentration of free heme. The presence of exogenous ALA bypasses the feedback control of this process, inducing the intracellular accumulation of photosensitizing concentrations of PpIX. A selective accumulation of PpIX occurs in areas of increased metabolism such as tumor cells.[12,15] The resulting tissue-specific photosensitization provides the basis for using ALA-induced PpIX for photodynamic diagnosis and therapy, whereby far lower light doses are used for photodynamic diagnosis. This technique has shown great promise in animal and human studies for head and neck cancers including oral lesions.[16–23] Limitations include the localization of induced fluorescence to the surface layers of the epithelium, and the fluorescence caused by common coexisting clinical pathologies such as candidal superinfection, hyperplasia, atrophy, ulceration.

1.1.3 Endogenous fluorescence

Another approach to fluorescence-based oral diagnosis uses endogenous emissions, or autofluorescence. One concept is the use of excitation and emission peaks at one specific set of wavelengths targeting specific fluorophores within the tissues and pathology-related changes that will affect fluorescence of these chromophores. While many authors have published extensive data on this approach, significant challenges include the low SNR, difficulty in quantifying data and in defining diagnostic milestones and endpoints, and limited tissue penetration.[23–26] Most studies were performed on small numbers of small biopsy samples, which do not necessarily translate directly or accurately to the clinical situation.

Other studies have measured fluorescence spectra in normal and neoplastic tissues.[27–36] Challenges are similar to those cited in the previous paragraph. Additionally, the abundance of data generated and our lack of complete understanding of the carcinogenesis process renders data analysis and interpretation very challenging. Localizing the exact source of the signal also can be difficult.

Precancers are characterized by epithelial changes including increased nuclear size, increased nuclear-to-cytoplasmic ratio, hyperchromasia, pleomorphism, angiogenesis, and increased metabolic rate.[37] Epithelial invasion of underlying structures with loss of basement membrane marks the transition to full-blown malignancy. The neoplastic process is associated with changes in the extracellular matrix (ECM), especially the collagen fibers and the framework that they constitute. Several authors have described collagen loss in early malignancy, although the time-resolved and spatially resolved sequence of this process remains undefined.[38] Angiogenesis and altered tissue perfusion and oxygenation also are implicated in neoplasia, but the specific sequential, spatial, and functional relationship between vascularization and neoplasia remains undefined. Thus, a noninvasive *in vivo* multimodal capability to image and characterize pathological oral changes at three levels—macroscopic, vascular, and cellular—should provide excellent diagnostic capability and advance our understanding of the sequential and spatial processes involved in oral carcinogenesis.

1.2 Optical Coherence Tomography (OCT) and Optical Doppler Tomography (ODT)

OCT is a new high-resolution optical technique that enables minimally invasive imaging of near-surface abnormalities in complex tissues. It has been compared to ultrasound scanning conceptually.[39] Both ultrasound and OCT provide real-time structural imaging, but unlike ultrasound, OCT is based on low-coherence interferometry, using broadband light to provide cross-sectional, high-resolution subsurface tissue images.[40,41] The engineering principles behind OCT have been described previously.[42–45] Broadband laser light waves are emitted from a source and directed toward a beamsplitter. One wave from the beamsplitter is sent toward a reference mirror with a known path length and the other toward the tissue sample. After the two beams reflect off the reference mirror and tissue sample surfaces at varying depths within the sample, the reflected light is directed back toward the beamsplitter, where the waves are recombined and read with a photodetector. The image is produced by analyzing interference of the recombined light waves. Cross-sectional images of tissues are constructed in real time, at near histologic resolution (approximately 10 μm with our current technology). This enables *in vivo* noninvasive imaging of the macroscopic characteristics of epithelial and subepithelial structures. While some research has reported ophthalmologic, dermatologic, gas-

trointestinal (GI), gynecological, cardiac, and other OCT applications,[46–71] the little research that has been reported in the oral cavity has focused predominantly on periodontal disease and hard tissue pathology.[69–71]

ODT combines Doppler velocimetry with OCT, resulting in extremely high resolution tomographic images of static and moving constituents such as blood in highly scattering biological tissues. Based on a phase-resolved technique, high spatial resolution and high-velocity sensitivity can be obtained simultaneously without compromising the image speed.

1.3 Multiphoton Excited Fluorescence (MPM)

MPM is a nonlinear, high-resolution optical method used in a variety of biological imaging applications.[72,73] The image-forming signal in MPM arises from the simultaneous interaction of two or more photons with the sample. Two-photon interactions in MPM result in second-harmonic generation (SHG) and two-photon excited fluorescence[74–77] (TPF). In TPF, two near-IR (NIR) wavelength photons are simultaneously absorbed, resulting in the emission of a longer wavelength photon.[78] TPF can be observed, depending on energy dissipation pathways of chromophores present in the examined specimens. Fluorescence spectra from two-photon absorption will not necessarily resemble spectra from linear spectroscopy. In SHG, the two NIR wavelength photons interact within the specimen to form a single photon of half the wavelength of the incident field.

Endogenous SHG in biological materials arises from the large molecular anisotropy and second-order nonlinear susceptibility typical of biological molecules and structures.[78] Collagen appears to be the tissue constituent mainly responsible[79,80] for SHG.

The goal of these studies was to use a combination of noninvasive optical *in vivo* technologies to test a multimodality approach to noninvasive diagnostics of oral premalignancy and malignancy.

2 Materials and Methods

Using the Golden Syrian Hamster (*Mesocricetus auratus*) cheek pouch model,[81] thrice weekly application of 0.5% DMBA (9,10 dimethyl-1,2-benzanthracene) in mineral oil to one cheek pouch produced dysplastic leukoplakia in 3 to 5 weeks, and squamous cell carcinoma after 8 to 12 weeks. Histological features in this model have been shown to correspond closely with premalignancy and malignancy in human oral mucosa.[81] The other cheek pouch was treated with mineral oil only and served as control. Noninvasive *in vivo* OCT/ODT and MPM/SHG were performed in hamsters by attaching the anesthetized hamster's everted cheek pouch to the microscope stage using a specially designed and fabricated ring-shaped clamp rigidly fastened to the stage surface. The clamping device was marked on its rim at 1-mm intervals to enable the use of localization coordinates for designating areas of specific interest and for achieving repeated, atraumatic scans with different modalities in exactly the same location. Accurate relocalization of the clamping device at weekly intervals was ensured by marking several coordinates of the device outline on the hamster cheek pouch using an animal microtattooing device (Ketchum lab animal micro tattooer, Ottawa, Canada). Three animals were sacrificed each week and tissues were subjected to routine sectioning and staining to provide parallel histopathology to the imaging data.

Histological evaluation of each stained section was quantified by two blinded, prestandardized scorers (one oral pathologist, one dentist) according to the criteria established by Macdonald,[82]. The following numerical grading system was used for each slide: 0—healthy, 1—hyperkeratosis, 2—mild dysplasia, 3—moderate dysplasia, 4—severe dysplasia, 5—carcinoma *in situ*, and 6—squamous cell carcinoma.

OCT diagnostic scores were based on changes in keratinization, epithelial thickening, epithelial proliferation and invasion, broadening of rete pegs, irregular epithelial stratification, and basal hyperplasia. Epithelial invasion was defined as loss of visible basement membrane. Each site was assessed for each of the preceding characteristics at a level of either none (0), slight (1), or marked (2). The score for each site depended on the range and severity of individual features and the proportion of epithelial thickness affected. Each scorer evaluated all data in one session once all data accrual was complete. OCT and hematoxylin and eosin (H&E) stained images were not paired in any way. A second reevaluation of all images by the same scorers in one session 3 months later was used to evaluate intraobserver variability.

MPM diagnosis was also scored using a scale of 0 to 6; H&E stained images were not paired with corresponding MPM images. MPM scores were based on collagen presence, structure, fiber length/organization, cellular exudates, vascularization, and microtumors. For collagen presence, fiber length, matrix structure, and organization as well as inflammatory exudates and presence of microtumors, changes were categorized as affecting percentages of image area: none, 1 to 25, 25 to 50, 51 to 75, and >75%. Vessel presence and location data were descriptive.

Finally, a combined diagnostic score designed to take advantage of the two imaging modalities was created by taking the average of the two OCT readings and two MPM readings, rounded to the nearest whole number.

3 Results and Discussion

Using *in vivo* OCT/ODT, we were able to image multiple epithelial and subepithelial layers as well as the presence or absence of basement membrane. Epithelial invasion during malignant transformation was clearly identified. Blood vessel presence, size, and localization relative to tumor tissue were visible, and blood flow could be quantified. In oral malignancy, small blood vessels were often seen in close proximity to tumor tissue.

Figures 1–3 show *in vivo* OCT (left) and H&E stained images (right) of healthy, dysplastic, and malignant hamster cheek pouch. In the OCT images, multiple epithelial and subepithelial layers and presence or absence of basement membrane are clearly visible. In the figures, the labels are 1, keratinized surface layer; 2, flat stratified squamous epithelium; 3, submucosa—dense fibrous connective tissue; 4, longitudinal striated muscle fiber; and 5, basement membrane.
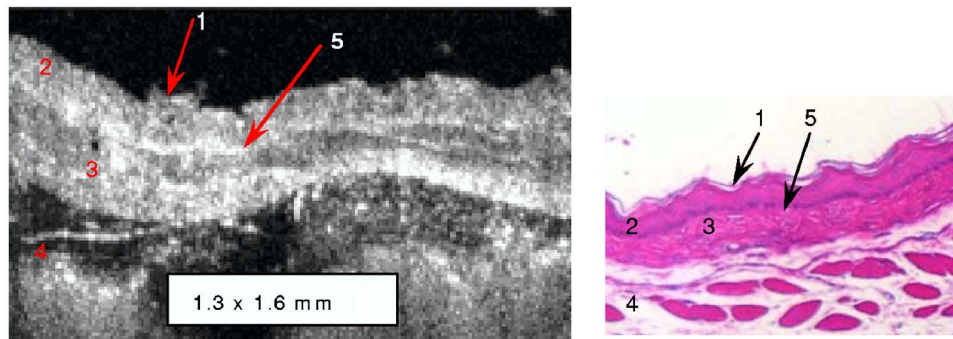
Fig. 1 H&E stained and *in vivo* OCT images of healthy hamster cheek pouch. In the OCT images, multiple epithelial and subepithelial layers and presence or absence of basement membrane are clearly visible: 1, keratinized surface layer; 2, flat stratified squamous epithelium; 3, submucosa: dense fibrous connective tissue; 4, longitudinal striated muscle fiber; and 5, basement membrane.

3.1 *Diagnostic Usefulness of OCT*

Intraobserver agreement for the two modalities (histopathology and OCT) at the two scoring time points was excellent. Using the kappa statistic for each of the two observers separately and for the observers combined, agreement was ⩾90% for each modality. The kappa statistic for OCT was 0.603 [standard error (SE)=0.091], indicating substantial agreement between observers based on the Brothwell standard scale of kappa significance in oral epithelial dysplasia.[82] "Substantial" spans kappa values from 0.61 to 0.80, lying between a "moderate" kappa of 0.41 to 0.60 and an "almost perfect" kappa of 0.81 to 1.00. This level of agreement can be elucidated as follows. For histopathology, there was perfect interobserver agreement between the two scores for any sample. For OCT, there was never a discrepancy of more than 1 point between scorers. Although the two observers disagreed in 12 of 35 cases, 25% of disagreements were between *in situ* carcinoma (5) and malignant (6), and 25% were between ratings of 0 and 1. Both these categories of discrepancy are minor with a low level of clinical relevance. In no case was there a disagreement between malignant (5 or 6) and nonmalignant (0 to 4), nor was any discrepancy more than 1 point.

OCT diagnosis agreed with histopathology for 56 of 70 (80%) readings (kappa=0.767, SE=0.056). Based on the Brothwell scale for oral epithelial dysplasia,[83] this kappa value is ranked as "substantial." Using OCT, the histopathology was underestimated by one category in six cases and overestimated in eight cases. In no instance was the difference between histopathology and OCT more than one level. Diagnostic sensitivity of OCT for differentiating between healthy (0 to 1) versus pathological (2 to 6) lesions was 0.98 (SE=0.020), and specificity was 0.95 (SE=0.049) if each score is considered separately ($n=70$). Using this technique, each sample is counted twice, as each sample was evaluated separately by each of the two scorers. Using the consensus score ($n=35$) from both investigators (in case of nonconsensus, the average of the two scores was used), sensitivity for OCT was 100% and specificity was 90%. Diagnostic sensitivity and specificity for differentiating between malignant (5 to 6) versus nonmalignant (0 to 4) lesions was 100%, and specificity was 96% (SE=0.028). Using the consensus score from both investigators (in case of nonconsensus, the higher of the two scores was used), sensitivity for OCT was 100% and specificity was 96%.

3.2 *MPM*

Noninvasive, atraumatic MPM and SHG imaging were possible *in vivo* throughout carcinogenesis in the hamster model at surface and subsurface levels within the tissues from
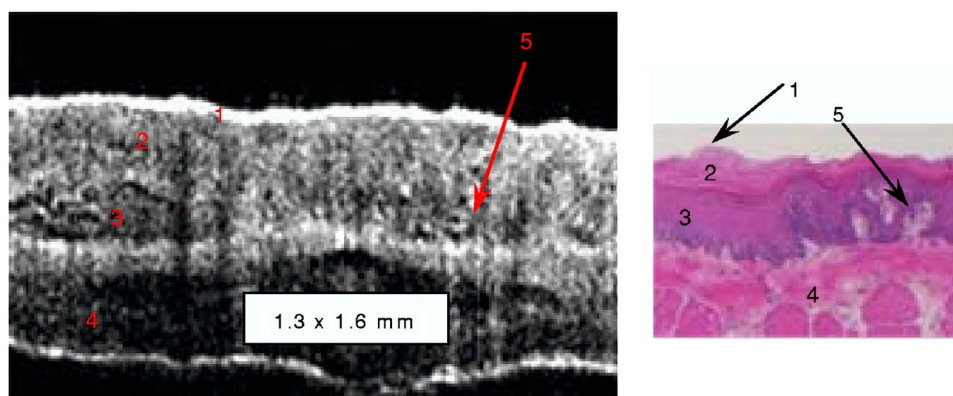

Fig. 2 H&E stained and *in vivo* OCT images of dysplastic hamster cheek pouch. In the OCT images, multiple epithelial and subepithelial layers and presence or absence of basement membrane are clearly visible: 1, keratinized surface layer; 2, flat stratified squamous epithelium; 3, submucosa: dense fibrous connective tissue; 4, longitudinal striated muscle fiber; and 5, basement membrane.
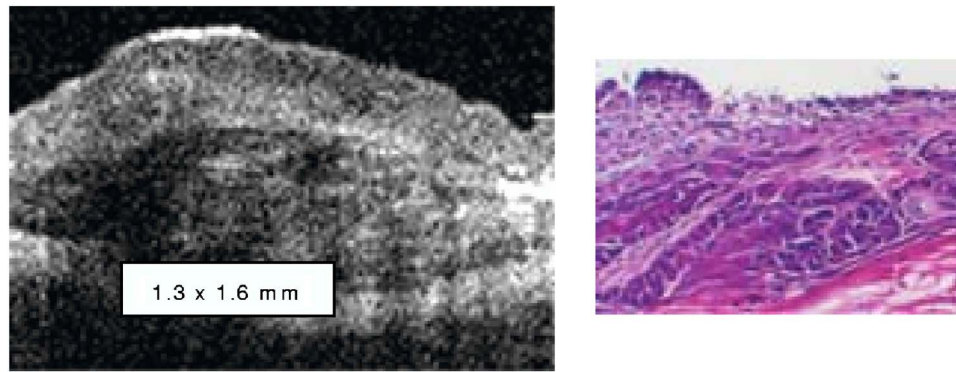
Fig. 3 H&E stained and *in vivo* OCT images of malignant hamster cheek pouch. In the OCT images, multiple epithelial and subepithelial layers and presence or absence of basement membrane are clearly visible.

0 to 900 μm depth. All of the images shown here were registered at a depth within the tissues of 700 to 800 μm. *In vivo* MPM clearly imaged a wide range of structural and functional characteristics. The presence and structure of the collagen/elastin framework were clearly visible, cellular infiltrates were apparent, normal versus engorged blood vessels could be identified, and microtumors were visualized. With the progression of carcinogenesis, the collagen matrix became increasingly disturbed, with reduced collagen fiber length and organization in the early dysplastic stages, followed by increasing loss of collagen fibers until, in squamous cell carcinoma, 40 to 60% of the ECM appeared to be devoid of a coherent collagen matrix. Cellular exudates developed, and finally microtumors became predominant as carcinogenesis progressed. Vascular change was most obvious during inflammation.

3.3 Diagnostic Usefulness of MPM

In this study, the diagnostic potential of MPM was compared with the histopathological gold standard. The same 35 animals and techniques were used as described in the preceding OCT/ODT section. Histological and MPM diagnosis of each sample were scored by two blinded, prestandardized investigators, as described for OCT. Again, diagnoses for both modalities were scored using a scale of 0 to 6; H&E stained images were not paired with corresponding MPM images. MPM scores were based on collagen presence, structure, fiber length/organization, cellular exudates, vascularization, and microtumors. For collagen presence, fiber length, matrix structure, and organization as well as inflammatory exudates and presence of microtumors, changes were categorized as affecting percentages of image area: none, 1 to 25, 25 to 50, 51 to 75, and >75%. Vessel presence and location data were descriptive.

Collagen fiber length and organization showed changes very early in the carcinogenesis process (2 to 3 weeks DMBA), whereas the onset of changes in the collagen presence occurred somewhat later (4 to 6 weeks). Cellular exudates were common throughout pathogenesis. In healthy tissue, a well-structured linear collagen matrix, with long, individual collagen fibers was seen consistently throughout the tissues. Blood vessels as well as cellular components within blood vessels were apparent. In inflamed tissues, engorged blood vessels were seen within an intact, but looser and less dense collagen matrix. Vessel presence and location appeared normal. Collagen fibrils appeared shorter, and the matrix demonstrated less of an interwoven structure. Typically, collagen presence was normal, but structure and organization were mildly altered in <25% of image area. Cellular infiltration was seen as diffuse patches of red autofluorescence in <25% of image area. The interstitial matrix was only partially intact in dysplastic tissues, with some areas of total collagen loss and other areas with variably reduced matrix structure and density. Typically, collagen presence, fiber length, and matrix structure were all reduced with increasing dysplasia severity. The collagen matrix presence and structure were altered in 25 to 75% of the image area. Collagen fibers that were present showed marked clumping. Blood vessels were occasionally engorged. Cellular exudates were seen throughout the tissues, typically affecting 25 to 50% of image area. Autofluorescence from microtumors was observed in malignant tissues. In early lesions, these were often very small, localized areas interspersed between remnants of collagen matrix. However, in tissues with advanced tumors, the collagen framework became disrupted to the point of complete disappearance and replacement by microtumors.

Intraobserver agreement for the two modalities (histopathology, MPM) at the two scoring time points ($t_1=0$, $t_2=3$ months) was excellent. Using the kappa statistic for each of the two observers separately and for the observers combined, intraobserver agreement was greater than 90% for each modality. With a kappa of 0.800 (SE=0.074), agreement between the two pathologists was at the top end of "substantial" on the Brothwell scale,[83] only one percentage point below "almost perfect."

MPM agreed with the histopathology for 62 of 70 (88.6%) readings. The MPM was underestimated by one category in three cases and overestimated in five cases. In no instance was the difference between histopathology and MPM more than one level. Using the kappa statistic, agreement between histopathology and MPM was "almost perfect" according to the Brothwell scale,[83] measuring 0.833 (SE=0.069) for observer 1, 0.900 (SE=0.055) for observer 2, and 0.867 (SE=0.044) for the observers combined.

Diagnostic sensitivity of MPM for differentiating between healthy (0 to 1) versus pathological (2 to 6) lesions was 98%

(SE=0.020) and specificity was 95% (SE=0.049) if each score was considered separately. Using this technique, each sample was counted twice, as each sample was evaluated separately by each of the two scorers. Using the consensus score from both investigators (in case of nonconsensus, the average of the two scores was used), sensitivity for MPM was 100% and specificity was 90%. Diagnostic sensitivity for differentiating between malignant (5 to 6) versus nonmalignant (0 to 4) lesions was 95% (SE=0.049) and specificity was 98% (SE=0.020). Using the consensus score from both investigators (in case of nonconsensus, the higher of the two scores was used), sensitivity for MPM was 100% and specificity was 96%. In the clinical situation, fluorescence from oral microbes can be observed.

3.4 *Combined OCT/MPM*

A combined diagnostic score designed to take advantage of the two imaging modalities was created by taking the average of the two OCT readings and two MPM readings, rounded to the nearest whole number. The combined OCT/MPM rating agreed with histopathology for 32 of 35 (91%) readings (kappa=0.900, SE=0.055). This level of agreement is considered "almost perfect" on the Brothwell scale for oral epithelial dysplasia.[83] Histopathology was overestimated by one category in each of three cases by the combined OCT/MPM score. Diagnostic sensitivity of OCT/MPM for differentiating between healthy (0 to 1) versus pathological (2 to 6) lesions was 100% and specificity was 90% (SE=0.49). Sensitivity for differentiating between malignant (5 to 6) and nonmalignant (0 to 4) lesions was 100% while specificity was 96% (SE=0.028). Both the kappa statistic and high sensitivity/specificity support the excellent imaging and diagnostic capabilities of the combined OCT/MPM approach.

4 Conclusion

OCT/ODT and MPM/SHG are promising noninvasive *in vivo* diagnostic modalities for oral dysplasia and malignancy.

References

1. *Cancer Facts and Figures*, p. 4, American Cancer Society, Washington, D.C. (2000).
2. J. Regezi and J. Sciubba, Eds., *Oral Pathology*, pp. 77–90, W.B. Saunders, Philadelphia (1993).
3. California Department of Health Services, "Cancer Surveillance Section Annual Report," (Mar. 1999).
4. D. P. Slaughter, H. W. Southwick, and W. Smejkal, "Field cancerization in oral stratified squamous epithelium," *Cancer* **6**, 963–968 (1953).
5. O. Kujan, A. M. Glenny, J. Duxbury, N. Thakker, and P. Sloan, "Evaluation of screening strategies for improving oral cancer mortality: a Cochrane systematic review," *J. Dent. Educ.* **69**(2), 255–265 (2005).
6. ADA Report of the ADA on Oral cancer, ADA, Chicago, Il (2002).
7. "Oral cancer," Report by the SMILE Foundation, Chicago, Il (2004).
8. J. B. Epstein, R. Feldman, R. J. Dolor, and S. R. Porter, "The utility of tolonium chloride rinse in the diagnosis of recurrent or second primary cancers in patients with prior upper aerodigestive tract cancer," *Head Neck* **25**(11), 911–921 (2003).
9. J. B. Epstein, L. Zhang, and M. Rosin, "Advances in the diagnosis of oral premalignant and malignant lesions," *J. Can. Dent. Assoc.* **68**(10), 617–621 (2002).
10. S. Silverman, C. Migliorati, and J. Barbosa, "Toluidine blue staining in the detection of oral precancerous and malignant lesions," *Oral Surg., Oral Med., Oral Pathol.* **57**, 379–382 (1984).
11. J. Epstein, C. Scully, and U. Spinelli, "Toluidine blue and Lugol's iodine solution for the assessment of oral malignant disease and lesions at risk of malignancy," *J. Oral Pathol. Med.* **21**, 160–163 (1992).
12. J. C. Kennedy and R. H. Pottier, "Endogenous protoporphyrin IX, a clinically useful photosensitizer for photodynamic therapy," *J. Photochem. Photobiol., B* **14**, 275–292 (1992).
13. R. C. J. Benson, "Treatment of diffuse transitional cell carcinoma in situ by whole bladder hematoporphyrin derivative photodynamic therapy," *J. Urol. (Baltimore)* **134**, 675–678 (1985).
14. Y. Hayata, H. Kato, C. Kanaka, J. Ono, and N. Takizawa, "Hematoporphyrin derivative and laser photoradiation in the treatment of lung cancer," *Chest* **81**, 269–277 (1982).
15. D. X. G. Divaris, J. C. Kennedy, and R. H. Poittier, "Phototoxic damage to sebaceous glands and hair follicles of mice after systemic administration of ALA correlates with localized PpIX fluorescence," *Am. J. Pathol.* **136**, 891–897 (1990).
16. K. Svanberg, I. Wang, R. Rydell, A. Elner, J. Wennerberg, L. Pais Clemente, E. Cardosa, R. Pratas, M. Pais Clemente, S. Andersson-Engels, and S. Svanberg, "Fluorescence diagnostics of head and neck cancer utilizing oral administration of δ-amino levulinic acid," *Proc. SPIE* **2371**, 129–141 (1995).
17. A. Ebihara, L.-H. Liaw, T. B. Krasieva, D. Messadi, K. Osann, and P. Wilder-Smith, "Detection and diagnosis of oral cancer by light-induced fluorescence," *Lasers Surg. Med.* **32**, 17–24 (2003).
18. A. Leunig, K. Rick, H. Stepp, R. Gutmann, G. Alwin, R. Baumgartner, and J. Feyh, "Fluorescence imaging and spectroscopy of 5-aminolevulinic acid-induced protoporphyrin IX for the detection of neoplastic lesions in the oral cavity," *Am. J. Surg.* **172**(6), 674–677 (1996).
19. B. Kulapaditharom and V. Boonkitticharoen, "Laser-induced fluorescence imaging in localization of head and neck cancers," *Ann. Otol. Rhinol. Laryngol.* **107**, 241–246 (1998).
20. W. Zenk, W. Dietel, P. Schleier, and S. Gunzel, "Visualizing carcinomas of the mouth cavity by stimulating synthesis of fluorescent protoporphyrin IX," *Mund Kiefer Gesichtschir* **3**(4), 205–209 (1999).
21. A. Leunig, C. S. Betz, M. Mehlmann, H. Stepp, G. Arbogast, and R. Baumgartner, "Detection of squamous cell carcinoma of the oral cavity by imaging 5-aminolevulinic acid-induced protoporphyrin IX fluorescence," *Laryngoscope* **110**, 78–83 (2000).
22. A. Leunig, M. Mehlmann, C. S. Betz, H. Stepp, G. Arbogast, G. Grevers, and R. Baumgartner, "Fluorescence staining of oral cancer using a topical application of 5-aminolevulinic acid: fluorescence microscopic studies," *Photochem. Photobiol.* **60**, 44–49 (2001).
23. C. S. Betz, H. Stepp, P. Janda, S. Arbogast, G. Grevers, R. Baumgartner, and A. Leunig, "A comparative study of normal inspection, autofluorescence and 5-ALA-induced PPIX fluorescence for oral cancer diagnosis," *Int. J. Cancer* **97**, 245–252 (2002).
24. G. Bottiroli, A. C. Corce, D. Locatelli, R. Marchesini, E. Pignoli, S. Tomatis, C. Cuzzoni, S. D. Palma, M. Dalfante, and P. Spinelli, "Natural fluorescence of normal and neoplastic human colon," *Lasers Surg. Med.* **16**, 48–60 (1995).
25. T. J. Romer, "Laser-induced fluorescence microscopy of normal colon and dysplasia in colonic adenomas," *Am. J. Gastroenterol.* **90**(1), 81–87 (1995).
26. A. Mahadevan, M. F. Mitchell, E. Silva, S. Thomsen, and R. R. Richard-Kortum, "A study of the fluorescence properties of normal and neoplastic human cervical tissue," *Lasers Surg. Med.* **13**, 647–655 (1993).
27. M. Ramajunam, M. F. Mitchell, A. Mahadevan, S. Thomsen, E. Silva, and R. R. Richards-Kortum, "Fluorescence spectroscopy: a diagnostic tool for CIN," *Gynecol. Oncol.* **52**, 32–38 (1994).
28. T. Vo-Dinh, M. Pamjehpour, B. F. Overholt, C. Farris, F. P. Bukley, and R. Sneed, "In vivo cancer diagnosis of the esophagus using DNF indices," *Lasers Surg. Med.* **16**, 41–47 (1995).
29. S. P. Schantz, V. Kolli, H. E. Savage, G. Yu, J. P. Shah, D. E. Harris,

A. Katz, R. R. Alfano, and A. G. Huvos, "In vivo native cellular fluorescence and histological characteristics of head and neck cancer," *Clin. Cancer Res.* **4**, 1177–1182 (1998).

30. A. Gillenwater, R. Jacob, B. Ganeshappa, B. Kemp, A. K. El-Naggar, J. L. Palmer, G. Clayman, M. F. Mitchell, and R. Richards-Kortum, "Noninvasive diagnosis of oral neoplasia based on fluorescence spectroscopy and native tissue autofluorescence," *Arch. Otolaryngol. Head Neck Surg.* **124**, 1251–1258 (1998).

31. C. T. Chen, C. Y. Wang, Y. S. Kuo, H. H. Chiang, S. N. Chow, I. Y. Hsiao, and C. P. Chiang, "Light-induced fluorescence spectroscopy," *Proc. Natl. Sci. Counc Repub China B* **20**, 123–130 (1996).

32. K. Roy, I. Bottrill, D. R. Ingrams, M. M. Pankratov, E. E. Rebeiz, P. Woo, S. Kabani, S. M. Shapshay, R. Manoharan, I. Itzkan, and M. S. Feld, "Diagnostic fluorescence spectroscopy of oral mucosa," *Proc. SPIE* **2395**, 135–142 (1995).

33. D. R. Ingrams, J. K. Dhingra, K. Roy, D. F. Perrault, Jr., I. D. Bottrill, S. Kabani, E. E. Rebeiz, M. M. Pankratov, S. M. Shapshay, R. Manoharan, I. Itzkan, and M. S. Feld, "Autofluorescence characteristics of oral mucosa," *Head Neck* **19**, 27–32 (1997).

34. C.-Y. Wang, H. K. Chiang, C.-T. Chen, C.-P. Chiang, Y.-S. Kuo, and S.-N. Chow, "Diagnosis of oral cancer by light-induced autofluorescence spectroscopy using double excitation wavelengths," *Oral Oncol.* **35**, 144–150 (1999).

35. M. B. Silberberg, H. E. Savage, G. C. Tang, P. G. Sacks, R. R. Alfano, and S. P. Schantz, "Detecting retinoic-acid induced biochemical alteration in squamous cell carcinoma using intrinsic fluorescence spectroscopy," *Laryngoscope* **104**, 278–282 (1994).

36. V. R. Kolli, A. R. Shaha, H. E. Savage, P. G. Sacks, M. A. Casale, and S. P. Schantz, "Native cellular fluorescence can identify changes in epithelial thickness in vivo in the upper aerodigestive tract," *Am. J. Surg.* **170**, 495–498 (1995).

37. I. Georgakoudi, B. C. Jacobsen, M. G. Mueller, E. E. Sheets, K. Badizadegan, D. L. Carr-Locke, C. P. Crum, C. W. Boone, R. R. Dasari, J. Van Dam, and M. S. Feld, "NAD(P)H and collagen as in vivo quantitative fluorescent biomarkers of epithelial precancerous changes," *Cancer Res.* **62**, 682–687 (2002).

38. M. Parikka, T. Kainulainen, K. Tasanen, A. Vaananen, L. Bruckner-Tudermann, and T. Salo, "Alterations of collagen XVII expression during transformation of oral epithelium to dysplasia and carcinoma," *J. Histochem. Cytochem.* **51**(7), 921–929 (2003).

39. P. J. Tadrous, "Methods for imaging the structure and function of living tissues and cells: I. Optical coherence tomography," *J. Pathol.* **191**(2), 115–119 (2000).

40. J. A. Izatt, M. D. Kulkarni, K. Kobayashi, M. V. Sivak, J. K. Barton, and A. J. Welch, "Optical coherence tomography for biodiagnostics," *Opt. Photonics News* **8**, 41–47 (1997).

41. Z. Ding, H. Ren, Y. Zhao, J. S. Nelson, and Z. Chen, "High-resolution optical coherence tomography over a large depth range with an axicon lens," *Opt. Lett.* **27**(4), 243–245 (2002).

42. D. Huang, E. A. Swanson, C. P. Lin, J. S. Schuman, W. G. Stinson, W. Chang, M. R. Hee, T. Flotte, K. Gregory, C. A. Puliafito, and J. G. Fujimoto, "Optical coherence tomography," *Science* **254**(5035), 1178–1181 (1991).

43. E. A. Swanson, J. A. Izatt, M. R. Hee, D. Huang, C. P. Lin, J. S. Schuman, C. A. Puliafito, and J. G. Fujimoto, "In vivo retinal imaging by optical coherence tomography," *Opt. Lett.* **18**(21), 1864–1866 (1993).

44. J. G. Fujimoto, "Biomedical imaging using optical coherent tomography," *Proc. SPIE* **3749**, 402–403 (1999).

45. B. Bouma, G. J. Tearney, S. A. Boppart, M. R. Hee, M. E. Brezinski, and J. G. Fujimoto, "High-resolution optical coherence tomographic imaging using a mode-locked Ti:Al2O3 laser source," *Opt. Lett.* **20**(13), 1486–1488 (1995).

46. P. Wilder-Smith, W. G. Jung, M. Brenner, K. Osann, H. Beydoun, D. Messadi, and Z. Chen, "Optical coherence tomography for the diagnosis of oral malignancy," *Lasers Surg. Med.* **35**, 269–275 (2004).

47. E. Matheny, R. Mina-Araghy, N. Hama, N. El-Abbadi, W. G. Jung, Z. Chen, P. Wilder-Smith, and M. Brenner, "Optical coherence tomography of malignancy in the hamster cheek pouch," *J. Biomed. Opt.* **9**(5), 978–981 (2004).

48. E. S. Matheny, N. Hanna, R. Mina-Araghi, W. G. Jung, Z. Chen, P. Wilder-Smith, and M. Brenner, "Optical coherence tomography of malignant hamster cheek pouches," *J. Investig. Med.* **51**(1), S78 (2003).

49. S. A. Boppart, M. R. Hee, J. G. Fumimoto, R. Birngruber, C. A. Toth, E. A. Swanson, et al., "Dynamic evolution and in vivo tomographic imaging of laser-induced retinal lesions by using optical coherence tomography," in *Proc. IEEE/CLEO*, pp. 17–14, Baltimore, MD (May 1995).

50. J. I. Youn, G. Vargas, B. J. Wong, and T. E. Milner, "Depth-resolved phase retardation measurements for laser-assisted non-ablative cartilage reshaping," *Phys. Med. Biol.* **50**(9), 1937–1950 (2005).

51. K. J. Bamford, S. W. James, H. Barr, and R. P. Tatam, "Optical low coherence tomography of bronchial tissue," in *Advanced Materials and Optical Systems For Chemical and biological detection*, *Proc. SPIE* **3858**, 172–179 (1999).

52. A. G. Bohorfoush, "New diagnostic methods for esophageal carcinoma," *Recent Results Cancer Res.* **155**, 55–62 (2000).

53. S. Brand, J. M. Ponero, B. E. Bouma, G. J. Tearney, C. C. Compton, and N. S. Nishioka, "Optical coherence tomography in the gastrointestinal tract," *Endoscopy* **32**(10), 796–803 (2000).

54. M. N. Menke, G. T. Feke, and C. L. Trempe, "OCT measurements in patients with optic disc edema," *Invest. Ophthalmol. Visual Sci.* **46**(10), 3807–3811 (2005).

55. V. Westphal, A. M. Rollins, J. Willis, M. V. Sivak, and J. A. Izatt, "Histology correlation with endoscopic optical coherence tomography," *Proc. SPIE* **3915**, 222–228 (2000).

56. Z. Chen, Y. Zhao, C. Saxer, S. Xiang, J. F. De Boer, and J. S. Nelson, "Phase-resolved OCT/ODT for imaging tissue microcirculation," *Proc. SPIE* **3915**, 413–414 (2000).

57. J. A. Izatt, M. D. Kulkami, S. Yazdanfar, J. K. Barton, and A. J. Welch, "In vivo bidirectional color Doppler flow imaging of picoliter blood volumes using optical coherence tomography," *Opt. Lett.* **22**(18), 1439–1441 (1997).

58. J. Kehlet Barton, J. A. Izatt, M. D. Kulkarni, S. Yazdanfar, and A. J. Welch, "Three-dimensional reconstruction of blood vessels from in vivo color Doppler optical coherence tomography images," *Dermatology* **198**(4), 355–361 (1999).

59. S. Yazdanfar, M. D. Kulkarni, and J. A. Izatt, "High resolution imaging of in vivo cardiac dynamics using color Doppler optical coherence tomography," *Opt. Express* **1**(13), 424–431 (1997).

60. S. Yazdanfar, A. M. Rollins, and J. A. Izatt, "In vivo imaging of blood flow in human retinal vessels using color Doppler optical coherence tomography," *Proc. SPIE Int. Soc. Opt. Eng.* **3598**, 117–185 (1999).

61. Z. Yonghua, Z. Chen, C. Saxer, X. Shaohua, J. F. de Boer, and J. S. Nelson, "Phase-resolved optical coherence tomography and optical Doppler tomography for imaging blood flow in human skin with fast scanning speed and high velocity sensitivity," *Opt. Lett.* **25**(2), 114–116 (2000).

62. P. Patwari, N. J. Weissman, S. A. Boppart, C. Jesser, D. Stamper, J. G. Fujimoto, and M. E. Brezinski, "Assessment of coronary plaque with optical coherence tomography and high-frequency ultrasound," *Am. J. Cardiol.* **85**(5), 641–644 (2000).

63. J. Perree, T. G. van Leeuwen, G. Pasterkamp, and J. A. Izatt, "Imaging of atherosclerotic plaques by optical coherence tomography (OCT)," *Proc. SPIE* **3915**, 522–527 (2000).

64. C. Pitris, S. A. Boppart, M. E. Brezinski, B. E. Bouma, and J. G. Fujimoto, "Cellular and neoplastic tissue imaging with optical coherence tomography," in *Proc. CLEO 1998*, pp. 127–128, Washington, D.C. (1998).

65. J. M. Poneros, S. Brand, B. E. Bouma, G. J. Tearney, C. C. Compton, and N. S. Nishioka, "Diagnosis of specialized intestinal metaplasia of the esophagus with optical coherence tomography," *Gastroenterology* **120**(1), 7–12 (2001).

66. J. M. Poneros, S. Brand, B. E. Bouma, G. J. Tearney, C. C. Compton, and N. S. Nishioka, "Diagnosis of specialized intestinal metaplasia by optical coherence tomography," *Gastroenterology* **120**(1), 7–12 (2001).

67. J. M. Poneros, G. J. Tearney, M. Shiskov, P. B. Kelsey, G. Y. Lauwers, N. S. Nishioka, and B. E. Bouma, "Optical coherence tomography of the biliary tree during ERCP," *Gastrointest Endosc* **55**(1), 84–88 (2002).

68. F. I. Feldchtein, G. V. Gelikonov, V. M. Gelikonov, R. V. Kuranov, A. M. Sergeev, N. D. Gladkova, et al., "Endoscopic applications of optical coherence tomography," *Opt. Express* **3**(6), 257–270 (1998).

69. B. W. Colston, M. J. Everett, L. B. DaSilva, L. L. Otis, P. Stroeve, and H. Nathel, "Imaging of hard and soft tissue in the oral cavity by optical coherence tomography," *Appl. Opt.* **37**(16), 3582–3585

(1998).

70. L. L. Otis, M. J. Everett, S. Sathyam, and B. W. Colston, "Optical coherence tomography: a new imaging technology for dentistry," *J. Am. Dent. Assoc.* **131**, 511–514 (2000).
71. B. W. Colston, M. J. Everett, U. S. Sathyam, L. B. DaSilva, and L. L. Otis, "Imaging of the oral cavity using optical coherence tomography," *Monogr. Oral Sci.* **17**, 32–55 (2000).
72. K. Konig, "Multiphoton microscopy in life sciences," *J. Microsc.* **200**, 83–104 (2000).
73. R. Williams, W. R. Zipfel, and W. W. Webb, "Multiphoton microscopy in biological research," *Curr. Opin. Chem. Biol.* **5**, 603–608 (2001).
74. E. Hecht, *Optics*, 3rd ed., Addison Wesley Longman, New York (1998).
75. B. E. A. Saleh and M. C. Teich, *Fundamentals of Photonics*, Wiley, New York (1991).
76. Y. R. Shen, *Principles of Nonlinear Optics*, Wiley, New York (1984).
77. P. J. Campagnola, M. D. Wei, A. Lewis, and L. M. Loew, "High-resolution nonlinear optical imaging of live cells by second harmonic generation," *Biophys. J.* **77**, 3341–3349 (1999).
78. R. Gauderon, P. B. Lukins, and C. J. Sheppard, "Optimization of second-harmonic generation microscopy," *Micron* **32**, 691–700 (2001).
79. W. R. Zipfel, R. M. Williams, and W. W. Webb, "Nonlinear magic: multiphoton microscopy in the biosciences," *Nat. Biotechnol.* **21**(11), 1369–1377 (2003).
80. W. F. Cheong, S. A. Prahl, and A. J. Welch, "A review of the optical properties of biological tissues," *IEEE J. Quantum Electron.* **26**(12), 2166–2185 (1990).
81. J. J. Salley, "Experimental carcinogenesis in the cheek pouch of the Syrian hamster," *J. Dent. Res.* **33**, 253–262 (1954).
82. D. G. MacDonald, "Comparison of epithelial dysplasia in hamster cheek pouch carcinogenesis and human oral mucosa," *J. Oral Pathol.* **10**, 186–191 (1981).
83. D. J. Brothwell, D. W. Lewis, G. Bradley, I. Leong, R. C. K. Jordan, D. Mock, and J. L. Leake, "Observer agreement in the grading of oral epithelial dysplasia," *Community Dent. Oral Epidemiol.* **31**(4), 300–305 (2003).
84. W. Denk, J. H. Strickler, and W. W. Webb, "Two photon laser scanning fluorescence microscopy," *Science* **248**(4951), 73–76 (1990).